A Comparative Study on the Electrical Properties of Vertical ($\bar{2}01$) and (010) β-Ga_2O_3 Schottky Barrier Diodes on EFG Single-Crystal Substrates

Houqiang Fu, *Student Member, IEEE*, Hong Chen, Xuanqi Huang, Izak Baranowski, Jossue Montes, Tsung-Han Yang, and Yuji Zhao, *Member, IEEE*

***Abstract*— This paper reports a comprehensive study on the anisotropic electrical properties of vertical ($\bar{2}01$) and (010) β-Ga_2O_3 Schottky barrier diodes (SBDs). The devices were fabricated on single-crystal substrates grown by an edge-defined film-fed growth method. The temperature-dependent current–voltage (I–V) and capacitance–voltage (C–V) characteristics were systematically measured, analyzed, and compared. The ($\bar{2}01$) and (010) SBDs exhibited on-resistances (R_{ON}) of 0.56 and 0.77 m$\Omega \cdot$ cm^2, turn-ON voltages (V_{ON}) of 1.0 and 1.3 V, Schottky barrier heights (SBHs) of 1.05 and 1.20 eV, electron mobilities of 125 and 65 cm^2/(V $\cdot$ s), respectively, with an on-current of $\sim$1.3 kA/cm^2 and on/off ratio of $\sim 10^9$. The (010) SBD had a larger V_{ON} and SBH due to anisotropic surface properties (i.e., surface Fermi level pinning and band bending), as supported by X-ray photoelectron spectroscopy measurements. Temperature-dependent I–V also revealed the inhomogeneous nature of the SBH in both devices, where the ($\bar{2}01$) SBD showed a more uniform SBH distribution. The homogeneous SBH was also extracted: 1.33 eV for the ($\bar{2}01$) SBD and 1.53 eV for the (010) SBD. The reverse leakage current of the devices was well described by the two-step trap-assisted tunneling model and the 1-D variable range hopping conduction model. The ($\bar{2}01$) SBD showed a larger leakage current due to its lower SBH and/or smaller activation energy, and thus a smaller breakdown voltage. These results indicate that the crystalline anisotropy of β-Ga_2O_3 can affect the electrical properties of vertical SBDs and should be taken into consideration when designing β-Ga_2O_3 electronics.**

***Index Terms*— Crystal anisotropy, gallium oxide, power electronics, Schottky barrier diodes (SBDs), semiconductor.**

I. Introduction

BETA-PHASE gallium oxide (β-Ga_2O_3) is a newly emerged candidate in the wide bandgap (WBG) semiconductor family, which has attracted considerable attention for efficient power conversion applications [1]–[3] in smart grids, renewable energy, data center power supply, and automotive electronics. Compared with other WBG semiconductors, such as SiC and GaN, β-Ga_2O_3 has larger bandgap E_g ($\sim$4.8 eV) and breakdown electric field E_{br} ($\sim$8 MV/cm) [4]–[6]. To evaluate the performance of power electronics, Baliga's figure of merit (FOM) ($\varepsilon_r \ \mu E_{br}^3$, where ε_r is the relative dielectric constant and μ is the mobility) is often used [6]. β-Ga_2O_3 exhibits a four times larger Baliga's FOM than SiC and GaN [5], [6], indicating that β-Ga_2O_3 power electronics have the potential to outperform SiC and GaN devices. One of the most important advantages of β-Ga_2O_3 is the availability of cost-effective single-crystal substrates [1]–[6]. Edge-defined film-fed growth (EFG) is one of the most popular methods for producing large-sized β-Ga_2O_3 substrates due to its low cost and compatibility with mass production [6]–[8]. High-quality 2-in ($\bar{2}01$) substrates grown by the EFG method have been commercialized with controllable doping concentrations ranging from 10^{16} to 10^{19} cm^{-3} and 4-in substrates have also been demonstrated [7], [9]. Substrates on other crystal orientations such as (010) [3], (100) [6], and (001) [10] can also be grown by an EFG method. Electronic devices on various crystal orientations have already been reported, such as FETs [1], [2] and Schottky barrier diodes (SBDs) [3], [6], [7], [10].

Because β-Ga_2O_3 has a highly asymmetric monoclinic crystal structure, the anisotropic material properties of β-Ga_2O_3 have garnered tremendous interest [11]–[14]. For example, Guo *et al.* [11] found a large anisotropy in the thermal properties of β-Ga_2O_3, where [010] direction had an approximately three times larger thermal conductivity than [100] direction. Chen *et al.* [12] observed anisotropic nonlinear optical properties such as the two-photon absorption coefficient and the Kerr refractive index on ($\bar{2}01$) and (010) β-Ga_2O_3. Wong *et al.* [13] reported electron mobility anisotropy in β-Ga_2O_3 FETs due to the anisotropic carrier scattering caused by asymmetric phonon modes [14]. In addition, evidence has also shown that the surface properties of β-Ga_2O_3 are also anisotropic due to different atomic configurations and dangling bonds on different orientations [15]–[17]. For example, Sasaki *et al.* [15] found the growth rate of (100) β-Ga_2O_3 was significantly lower

Manuscript received April 13, 2018; accepted May 26, 2018. Date of publication June 8, 2018; date of current version July 23, 2018. The review of this paper was arranged by Editor H. Wong. *(Corresponding author: Yuji Zhao.)*

The authors are with the School of Electrical, Computer, and Energy Engineering, Arizona State University, Tempe, AZ 85287 USA (e-mail: houqiang@asu.edu; yuji.zhao@asu.edu).

Color versions of one or more of the figures in this paper are available online at http://ieeexplore.ieee.org.

Digital Object Identifier 10.1109/TED.2018.2841904

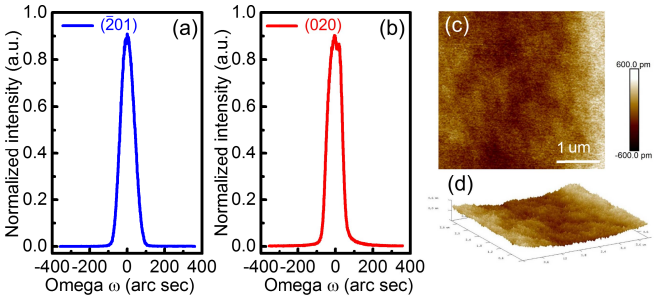

Fig. 1. RCs by HRXRD for (a) $(\bar{2}01)$ and (b) (010) β-Ga_2O_3 substrates. Representative AFM images of the two substrates in (c) two dimensions and (d) three dimensions.

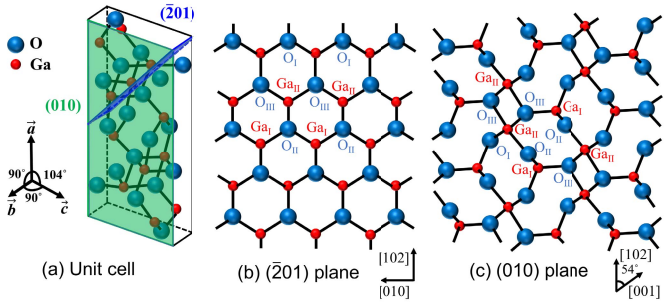

Fig. 2. (a) Unit cell of β-Ga_2O_3 crystal with $(\bar{2}01)$ and (010) planes labeled. The atomic structures of (b) $(\bar{2}01)$ plane and (c) (010) plane.

than other orientations due to the low adhesion energy on the terraces of the (100) surface. Hogan *et al.* [16] studied the dry etching of β-Ga_2O_3 by inductively coupled plasma (ICP) and obtained much lower etching rate on (100) than on (010) and $(\bar{2}01)$ due to the surface oxygen anions and lower dangling bond density. Similar anisotropic etch rates were also observed in the KOH wet etching of β-Ga_2O_3 [17].

From a device perspective, these anisotropic bulk and surface material properties of β-Ga_2O_3 are expected to have an impact on the performances of β-Ga_2O_3 electronic devices. Similar phenomena have already been observed in wurtzite III-nitride semiconductors, where devices grown on polar, semipolar, and nonpolar orientations have shown distinct behaviors [18]–[21]. However, systematic and comparative study on the effect of crystalline anisotropy on the β-Ga_2O_3 electronic devices is still lacking. In this paper, we fabricated vertical $(\bar{2}01)$ and (010) β-Ga_2O_3 SBDs on EFG single-crystal substrates with similar material qualities and comprehensively compared their electrical properties. The crystal orientations and associated surface properties do impact the behaviors of the SBDs at both forward and reverse biases in terms of turn-ON voltage (V_{ON}), Schottky barrier height (SBH), electron mobility, and reverse leakage current and breakdown voltage.

II. Material Characterization and Device Fabrication

The β-Ga_2O_3 single-crystal substrates were grown by an EFG method. High-purity Ga_2O_3 powder was the source material and tin oxide (SnO_2) powder was the precursor for n-type Sn dopants. The powder mixture was melted by radio frequency heating, after which a β-Ga_2O_3 seed crystal was used to initialize the crystal growth. More information about the growth methods can be found elsewhere [8]. The $(\bar{2}01)$ and (010) substrates had the similar doping concentration. The crystal quality of the substrates was characterized by PANalytical X'Pert Pro high-resolution X-ray diffraction (HRXRD) using Cu Kα1 radiation with a wavelength of 1.541 Å. Hybrid monochromator and triple axis module were used as incident and diffracted beam optics, respectively. Fig. 1(a) and (b) presents the rocking curves (RCs) for the $(\bar{2}01)$ and (010) β-Ga_2O_3 substrates, respectively. The full-width at half-maximum (FWHM) of the $(\bar{2}01)$ RC was 87 arcsec and the FWHM of the (020) RC was 90 arcsec. This indicates that both substrates have similar crystal quality with a dislocation density of $\sim 10^7$ cm^{-2} based on the methods described in [22]. Bruker's multimode atomic force microscopy (AFM) was used to examine the surface morphology of the substrates and the representative images of both substrates were shown in Fig. 1(c) and (d). The root-mean-square roughness of the 4×4 μm^2 scanning area of the two substrates was 0.1–0.2 nm. HRXRD and AFM results indicate high-quality β-Ga_2O_3 substrates with low dislocation density and good surface morphology were obtained.

Fig. 2 shows the schematic unit cell of β-Ga_2O_3 and atomic configurations of $(\bar{2}01)$ and (010) planes [16], [17], [23]. β-Ga_2O_3 crystallizes into a monoclinic structure ($C2/m$) with lattice constants $a = 1.223$ nm, $b = 0.304$ nm, and $c = 0.580$ nm and angles $\alpha = \gamma = 90°$ and $\beta = 104°$. There are two gallium sites: tetrahedrally coordinated Ga_I (four bonds) and octahedrally coordinated Ga_{II} (six bonds), and three oxygen sites: O_I (three bonds), O_{II} (three bonds), and O_{III} (four bonds). $(\bar{2}01)$ and (010) surfaces differ significantly in atomic configurations and dangling bonds. The $(\bar{2}01)$ surface is exclusively terminated either by Ga_I or Ga_{II} or oxygen, while the (010) surface is composed of both gallium (Ga_I and Ga_{II}) and oxygen with a Ga-to-O ratio of 2:3 [16], [17]. To assess the surface properties of the $(\bar{2}01)$ and (010) substrates, X-ray photoelectron spectroscopy (XPS) measurements were carried out using a monochromated Al Kα X-ray source under an ultrahigh vacuum of $<10^{-9}$ torr. The system was calibrated by the standard reference C 1s peak. The valance band (VB) minimum (E_{VBM}) can be extracted by linearly extrapolating the leading edge of the VB spectra to the baseline, as shown in Fig. 3. The procedure of calculating surface band bending of semiconductors is detailed in [24]. In n-type semiconductors, due to surface states and defects, the Fermi level is pinned at the charge neutrality level at the surface, where the surface barrier height Φ_{surf} is given by [24]

$$\Phi_{surf} = E_g - E_{VBM}. \quad (1)$$

The obtained Φ_{surf} was 1.14 eV for the $(\bar{2}01)$ surface and 1.63 eV for the (010) surface. The conduction bands (CBs) were bent upward, indicating the presence of negatively charged surface states and defects at the surfaces [24]. This is partly responsible for the difficulty in forming ohmic contacts to β-Ga_2O_3 [1], [6]. The (010) surface has a 0.49 eV larger band bending, which explains the fact that

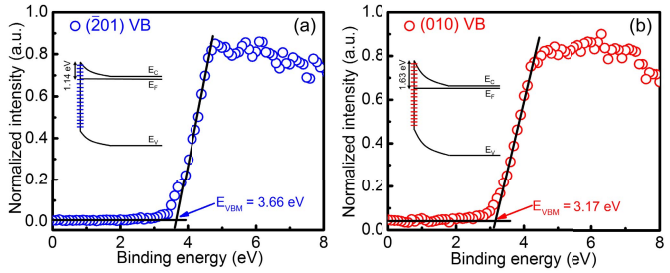

Fig. 3. XPS valence band spectra of (a) ($\bar{2}01$) and (b) (010) β-Ga_2O_3. E_{VBM} values were also extracted by extrapolation. Insets: upward band bending at the surfaces.

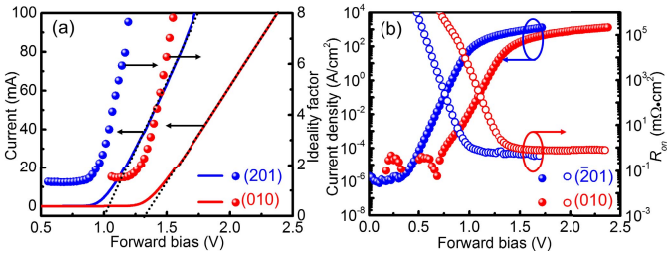

Fig. 4. (a) Current and ideality factor as a function of forward bias in linear scale. The V_{ON} values were also obtained by linear extrapolation. (b) Current density and R_{ON} versus forward bias in semilog scale.

it is more difficult to realize ohmic contacts on the (010) orientation [1], [2], [17], [25]. The different crystal structures and surface properties of ($\bar{2}01$) and (010) β-Ga_2O_3 could impact the electrical properties of devices based on them. Section III will use β-Ga_2O_3 vertical SBDs as a case study and comprehensively compare their device performances.

The SBDs were fabricated on the ($\bar{2}01$) and (010) β-Ga_2O_3 substrates using optical photolithography. The two substrates were cleaned in acetone and isopropyl alcohol. The backside surfaces of the substrates were treated by the BCl_3-based ICP etching for 5 min at an ICP source/bias power of 400/30 W, a BCl_3/Ar flow rate of 20/5 sccm, and a pressure of 15 mtorr [16]. The etch rate was ~20 nm/min and the total etching thickness was ~100 nm. The etching process can create donor-like surface defects to facilitate ohmic contacts [1], [6]. For ohmic contacts, Ti/Al/Ti/Au metal stacks were formed on the backside of the substrates using electron beam evaporation, followed by rapid thermal annealing (RTA) at 470 °C in nitrogen for 1 min. For the circular Schottky contacts (diameter of 100 μm), Pt/Au metal stacks were deposited by electron beam evaporation. The electrical measurements were carried out on a probe station with a controllable thermal chuck. The current–voltage (I–V) characteristics were obtained using the Keithley 2410 sourcemeter. The capacitance–voltage (C–V) characteristics were measured by the Keithley 4200-SCS parameter analyzer.

III. Results and Discussion

Fig. 4(a) shows the forward I–V characteristics of the ($\bar{2}01$) and (010) SBDs at room temperature (RT) in linear scale. The measurement apparatus has an upper current limit of 0.1 A. The forward current of the devices exceeded 0.1 A at a voltage

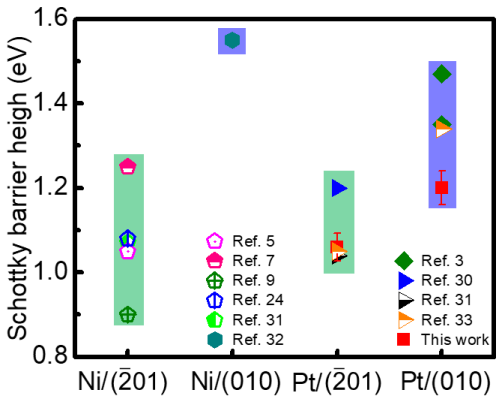

Fig. 5. Comparison of SBHs of ($\bar{2}01$) and (010) β-Ga_2O_3 SBDs.

of 1.7 V in the ($\bar{2}01$) SBD and 2.4 V in the (010) SBD. V_{ON} values of ($\bar{2}01$) and (010) SBDs were (1.0 ± 0.05) and (1.3 ± 0.1) V, respectively. The ideality factor n can be calculated as a function of voltage by [26], [27]

$$n = \frac{q}{2.3\ kT}\frac{1}{d(\log I)/dV} \tag{2}$$

where q is the electron charge, k is Boltzmann's constant, T is the temperature, and I is the current. At low bias, n was 1.34 and 1.55 for the ($\bar{2}01$) SBD and the (010) SBD, respectively. Fig. 4(b) presents current density and differential specific R_{ON} of the SBDs as a function of voltage in semilog scale. Both SBDs showed a high ON-current of ~1.3 kA/cm^2 and ON/OFF ratio of ~10^9, which are among the highest values reported in vertical β-Ga_2O_3 SBDs [3], [6], [28]. At 1.3 kA/cm^2, R_{ON} was 0.56 and 0.77 m$\Omega \cdot$ cm^2 for ($\bar{2}01$) and (010) SBDs, respectively. μ of the SBDs can be extracted by $t/qN_D R_{ON}$, where t is the substrate thickness and N_D is the carrier concentration, considering a negligibly small contact resistance [26], [27]. It is worth noting that high current densities can lead to ~10 μm of current spreading from the Schottky contact [29], which leads to an increase in the effective contact area. Taking these current spreading effects into consideration, the electron mobility was calculated to be 125 cm^2/(V $\cdot$ s) for the ($\bar{2}01$) SBD and 65 cm^2/(V $\cdot$ s) for the (010) SBD, which are comparable to previous reports [7], [9], [13]. The difference in the electron mobilities of the two devices is possibly due to anisotropic electron transport properties of β-Ga_2O_3 [13], [14].

The I–V characteristics of the SBDs can be described by the thermionic emission model [10]

$$J = A^* T^2 \exp(-q\Phi_B/kT)[\exp(qV/nkT) - 1] \tag{3}$$

where J is the current density, A^* is the Richardson constant, and Φ_B is the SBH. A^* was calculated to be 41.1 A/(cm^2 K^2) using an effective electron mass of 0.34 m_0 [3]. The extracted SBH was 1.05 eV for the ($\bar{2}01$) SBD and 1.20 eV for the (010) SBD. Fig. 5 shows that (010) SBDs generally have higher SBH than ($\bar{2}01$) SBDs, which is consistent with previous reports [3], [5], [7], [9], [25], [30]–[33], and the larger Φ_{surf} of the (010) surface according to the XPS results (see Fig. 3). It has already been shown that the SBH of β-Ga_2O_3 SBDs

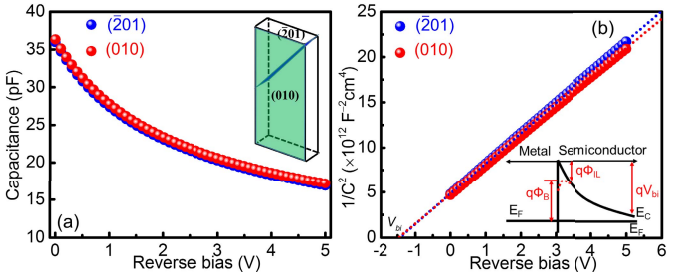

Fig. 6. (a) C–V and (b) $1/C^2$–V characteristics of ($\bar{2}01$) and (010) SBDs at 1 MHz. The inset in (b) shows the band diagram of Pt/β-Ga_2O_3 Schottky interface.

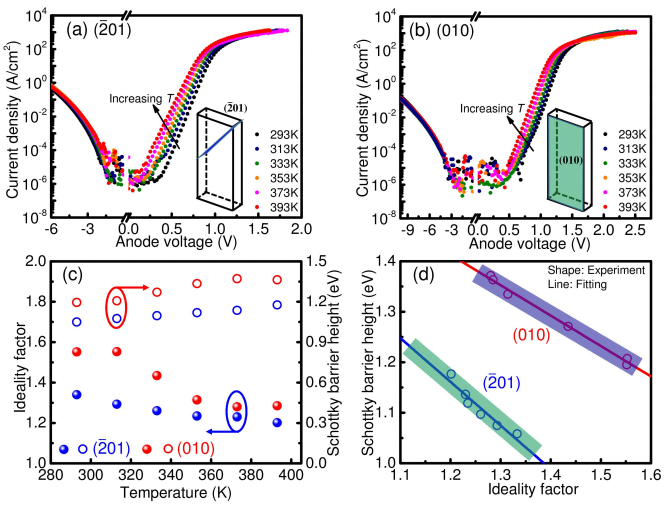

Fig. 7. Temperature-dependent I–V characteristics for (a) ($\bar{2}01$) SBD and (b) (010) SBD. (c) Ideality factor and SBH as a function of temperature for the two devices. (d) SBH versus ideality factor.

is more dominated by the surface states and defects than by the actual metal used [31], [33]. As shown in Figs. 2 and 3, the ($\bar{2}01$) and (010) surfaces have distinct Fermi level pinning and band bending. This indicates that the interface states and defects between metal/β-Ga_2O_3 are different for ($\bar{2}01$) and (010) SBDs, leading to the discrepancy in the SBH between the two devices. In addition, we also observed the difference in the SBH between this paper and [3], [30], and [33]. This may be caused by different crystal qualities (i.e., defect densities) and/or surface morphologies (i.e., surface roughness) and/or surface treatments before metal depositions.

Fig. 6 shows the C–V and $1/C^2$–V characteristics of the ($\bar{2}01$) and (010) SBDs at a frequency of 1 MHz and RT. The built-in voltage V_{bi} can be extracted from the intercept of $1/C^2$ versus V by [10], [34]

$$1/C^2 = \frac{2}{q\varepsilon_0\varepsilon_r N_D}(V_{bi} - V - kT/q) \tag{4}$$

where ε_0 is the permittivity of the vacuum. V_{bi} of the ($\bar{2}01$) SBD was 1.41 V and that of the (010) SBD was 1.44 V. As shown in the inset of Fig. 5(b), the SBH can be expressed as [10]

$$q\Phi_B = qV_{bi} - q\Phi_{\mathrm{IL}} + (E_C - E_F) \tag{5}$$

where Φ_{IL} is the image-force-induced barrier height lowering, E_C is the CB minimum, and E_F is the Fermi level. Φ_{IL} is given by [10]

$$q\Phi_{\mathrm{IL}} = \sqrt{qE_{\mathrm{SBD}}/(4\pi\varepsilon_0\varepsilon_r)} \tag{6}$$

$$E_{\mathrm{SBD}} = \sqrt{2qN_D V_{bi}/(\varepsilon_0\varepsilon_r)} \tag{7}$$

where E_{SBD} is the electric field at the metal/semiconductor interface. $(E_C - E_F)$ is calculated by $kTln(N_C/N_D)$, where N_C is the effective density states. N_D was obtained from the slope of (4): 4.2×10^{18} cm^{-3} for the ($\bar{2}01$) SBD and 4.3×10^{18} cm^{-3} for the (010) SBD. After plugging in all the terms into (5), the SBH was (1.27 ± 0.01) eV for ($\bar{2}01$) SBD and (1.30 ± 0.01) eV for (010) SBD. Φ_B values obtained from I–V are smaller than those from C–V for both devices. This is usually attributed to the spatially inhomogeneous SBH caused by the interfacial states and defects between metal/semiconductor [33], [35]–[37]. Furthermore, Φ_B of two SBDs from the C–V data has only a small difference of 0.03 eV compared with 0.15-eV Φ_B difference from the I–V data. The C–V SBH is more influenced by the doping concentrations of the semiconductors and does not involve current conduction, while the I–V SBH represents the barrier height for current flow [33]. Therefore, the C–V SBH is insensitive to the crystal orientations and surface properties of β-Ga_2O_3 that dominate the current conduction.

Fig. 7(a) and (b) presents the temperature-dependent I–V characteristics for the ($\bar{2}01$) and (010) SBDs. Based on (3), the SBH and ideality factor of the devices were extracted as a function of temperature shown in Fig. 7(c). For the ($\bar{2}01$) SBD, Φ_B increased from 1.05 to 1.18 eV and n decreased from 1.34 to 1.20 with increasing temperature. For the (010) SBD, Φ_B increased from 1.20 to 1.36 eV and n decreased from 1.55 to 1.29 with increasing temperature. The temperature dependence of the ideality factor, also called "T_0 anomaly," is caused by the spatial inhomogeneity of SBH as a result of surface states and defects at the metal/semiconductor interface [36], as confirmed by the previous XPS results. Similar phenomena have also been observed in other semiconductors [36], [37]. The ideality factor can be described as a function of temperature by [36]

$$n = 1 + T_0/T \tag{8}$$

where T_0 is a constant associated with the standard deviation of the SBH distribution. Fitting experimental data with (8) yielded T_0 of 88 K for the ($\bar{2}01$) SBD and T_0 of 133 K for the (010) SBD. The smaller T_0 of the ($\bar{2}01$) SBD indicates a more uniform SBH distribution due to different surface properties. In Fig. 7(d), there was a well-known linear relationship between the SBH and ideality factor for both devices due to the inhomogeneous Schottky barrier interfaces [34], [36]. By extrapolation, the homogenous SBH ($\Phi_{B,I-V,h}$) when $n = 1$ was 1.33 eV for the ($\bar{2}01$) SBD and 1.53 eV for the (010) SBD, which are larger than their inhomogeneous SBH ($\Phi_{B,I-V,ih}$ = 1.05 and 1.20 eV, respectively). The device performance metrics of the two devices from forward I–V and C–V characteristics are summarized in Table I.

TABLE I
SUMMARY OF DEVICE PARAMETERS FOR THE ($\bar{2}01$) AND (010) SBDS

Sample	R_{on} ($m\Omega\cdot cm^2$)	V_{on} (V)	n	Mobility [$cm^2/(V\cdot s)$]	$\Phi_{B,\,I\text{-}V,\,ih}$ (eV)	$\Phi_{B,\,I\text{-}V,\,h}$ (eV)	$\Phi_{B,\,C\text{-}V}$ (eV)
($\bar{2}01$)	0.56	1.0	1.34	125	1.05	1.33	1.27
(010)	0.77	1.3	1.55	65	1.20	1.53	1.30

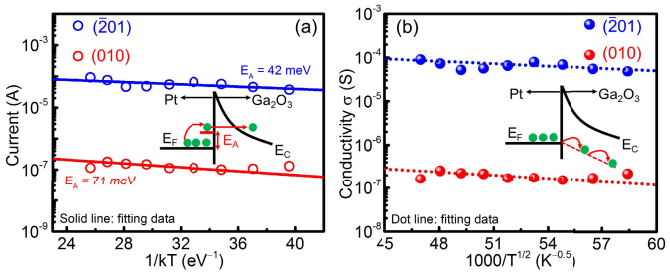

Fig. 8. (a) Arrhenius plot of reverse leakage current of the two SBDs with activation energy extracted. Inset: electron transport in two-step trap-assisted tunneling model. (b) Conductivity as a function of $1/T^{1/2}$ for the two SBDs. The 1D-VRH conduction model (dotted line) is used to fit the data. Inset: electron transport in this model.

Fig. 8 shows the experimental and theoretical data of temperature-dependent reverse leakage current of the two SBDs at −6 V. The reverse leakage current of SBDs above RT is usually characterized by two models [38]. The first model is the two-step trap-assisted tunneling mechanism, where the electrons in the metal first are thermally excited to the trap states and then tunnel through the Schottky barrier [shown in the inset of Fig. 8(a)]. The reverse leakage current is proportional to $exp(-E_A/kT)$, where E_A is the activation energy, which is the energy difference between the Fermi level and the trap states. Good agreement was obtained between the experiment and this model in the Arrhenius plot in Fig. 8(a). E_A was 42 meV for the ($\bar{2}01$) SBD and 71 meV for the (010) SBD, which are comparable to previous results [39]. Another possible model is the 1-D variable-range-hopping (1D-VRH) conduction model, where the electrons in the metal first fall into defect states associated with a dislocation near or below the Fermi level and are then transported into the semiconductor by hopping conduction [shown in the inset of Fig. 8(b)]. In this model, the conductivity is given by [38]

$$\sigma = \sigma_0 \exp[-(T_1/T)^{1/2}] \tag{9}$$

where T_1 is the characteristic temperature and σ_0 is a fitting parameter whose value is the conductance at temperatures $\gg T_1$. Fig. 8(b) shows a good linear fitting for the log of the conductivity as a function of $1/T^{1/2}$ between experimental and simulation data. It is not yet clear which model is the dominant mechanism based on current data and further investigations are undergoing. In addition, the ($\bar{2}01$) SBD exhibited higher reserve leakage current than the (010) SBD, which can be attributed to lower SBH and/or smaller E_A of the ($\bar{2}01$) SBD. The breakdown voltage of the ($\bar{2}01$) SBD was ∼15 V and that of the (010) SBD was ∼25 V. Please be noted that both devices have high doping concentrations and their breakdown voltages are, therefore, relatively low. The (010) SBD had a larger breakdown voltage than the ($\bar{2}01$) SBD, which is consistent with the fact that the ($\bar{2}01$) SBD had a larger leakage current than the (010) SBD.

IV. CONCLUSION

Vertical β-Ga_2O_3 SBDs were fabricated on single-crystal ($\bar{2}01$) and (010) substrates grown by the EFG method, followed by comprehensive device analysis. The devices showed excellent forward characteristics with a record low R_{ON}, a high ON-current, and a high electron mobility. The ($\bar{2}01$) SBD showed smaller V_{ON} and SBH than the (010) SBD, attributed to anisotropic crystal structure and surface properties, as confirmed by XPS results. Temperature-dependent I–V characteristics revealed the inhomogeneous nature of the SBH for both devices, where the ($\bar{2}01$) SBD exhibited a more uniformly distributed SBH. The reverse leakage current of both devices was simulated by the two-step trap-assisted tunneling model and the 1D-VRH model. Good agreements between experimental and theoretical data were obtained for both models. Further investigation is demanded to determine the dominant mechanism. In addition, the ($\bar{2}01$) SBD showed a larger reverse leakage current and smaller breakdown voltage than the (010) SBD. This paper shows that the crystalline anisotropy of β-Ga_2O_3 can impact the electrical properties of vertical SBDs, and possibly transistors as well. Special attention needs to be paid to the anisotropic electrical properties when designing β-Ga_2O_3 electronics.

ACKNOWLEDGMENT

The authors would like to thank the use of facilities within the LeRoy Eyring Center for Solid State Science at Arizona State University. They would like to Tamura Corporation for providing the samples. The device fabrication was done in the Center for Solid State Electronics Research at Arizona State University.

REFERENCES

[1] M. Higashiwaki, K. Sasaki, A. Kuramata, T. Masui, and S. Yamakoshi, "Gallium oxide (Ga_2O_3) metal-semiconductor field-effect transistors on single-crystal β-Ga_2O_3(010) substrates," *Appl. Phys. Lett.*, vol. 100, no. 1, p. 013504, Jan. 2012.

[2] M. Higashiwaki *et al.*, "Depletion-mode Ga_2O_3 metal-oxide-semiconductor field-effect transistors on β-Ga_2O_3(010) substrates and temperature dependence of their device characteristics," *Appl. Phys. Lett.*, vol. 103, no. 12, p. 123511, Sep. 2013.

[3] K. Sasaki, M. Higashiwaki, A. Kuramata, T. Masui, and S. Yamakoshi, "Ga_2O_3 Schottky barrier diodes fabricated by using single-crystal β–Ga_2O_3(010) substrates," *IEEE Electron Device Lett.*, vol. 34, no. 4, pp. 493–495, Apr. 2013.

[4] H. H. Tippins, "Optical absorption and photoconductivity in the band edge of β-Ga_2O_3," *Phys. Rev.*, vol. 140, no. 1A, pp. 316–319, Oct. 1965.

[5] Z. Zhang, E. Farzana, A. R. Arehart, and S. A. Ringel, "Deep level defects throughout the bandgap of (010) β-Ga_2O_3 detected by optically and thermally stimulated defect spectroscopy," *Appl. Phys. Lett.*, vol. 108, no. 5, p. 052105, Feb. 2016.

[6] Q. He *et al.*, "Schottky barrier diode based on β-Ga_2O_3(100) single crystal substrate and its temperature-dependent electrical characteristics," *Appl. Phys. Lett.*, vol. 110, no. 9, p. 093503, Mar. 2017.

[7] T. Oishi, Y. Koga, K. Harada, and M. Kasu, "High-mobility β-$Ga_2O_3(\bar{2}01)$ single crystals grown by edge-defined film-fed growth method and their Schottky barrier diodes with Ni contact," *Appl. Phys. Express*, vol. 8, no. 3, p. 031101, Feb. 2015.

[8] A. Kuramata, K. Koshi, S. Watanabe, Y. Yamaoka, T. Masui, and S. Yamakoshi, "High-quality β-Ga_2O_3 single crystals grown by edge-defined film-fed growth," *Jpn. J. Appl. Phys.*, vol. 55, no. 12, p. 1202A2, Nov. 2016.

[9] T. Oishi, K. Harada, Y. Koga, and M. Kasu, "Conduction mechanism in highly doped β-$Ga_2O_3(\bar{2}01)$ single crystals grown by edge-defined film-fed growth method and their Schottky barrier diodes," *Jpn. J. Appl. Phys.*, vol. 55, no. 3, p. 030305, Feb. 2016.

[10] M. Higashiwaki *et al.*, "Temperature-dependent capacitance–voltage and current–voltage characteristics of Pt/Ga_2O_3(001) Schottky barrier diodes fabricated on n–Ga_2O_3 drift layers grown by halide vapor phase epitaxy," *Appl. Phys. Lett.*, vol. 108, no. 13, p. 133503, Mar. 2016.

[11] Z. Guo *et al.*, "Anisotropic thermal conductivity in single crystal β-gallium oxide," *Appl. Phys. Lett.*, vol. 106, no. 11, p. 111909, Mar. 2015.

[12] H. Chen *et al.*, "Characterizations of the nonlinear optical properties for (010) and $(\bar{2}01)$ beta-phase gallium oxide," *Opt. Express*, vol. 26, no. 4, pp. 3938–3946, Feb. 2018.

[13] M. H. Wong, K. Sasaki, A. Kuramata, S. Yamakoshi, and M. Higashiwaki, "Electron channel mobility in silicon-doped Ga_2O_3 MOSFETs with a resistive buffer layer," *Jpn. J. Appl. Phys.*, vol. 55, no. 12, p. 1202B9, Oct. 2016.

[14] M. Schubert *et al.*, "Anisotropy, phonon modes, and free charge carrier parameters in monoclinic β-gallium oxide single crystals," *Phys. Rev. B, Condens. Matter*, vol. 93, no. 12, p. 125209, Mar. 2016.

[15] K. Sasaki, A. Kuramata, T. Masui, E. G. Víllora, K. Shimamura, and S. Yamakoshi, "Device-quality β-Ga_2O_3 epitaxial films fabricated by ozone molecular beam epitaxy," *Appl. Phys. Express*, vol. 5, no. 3, p. 035502, Feb. 2012.

[16] J. E. Hogan, S. W. Kaun, E. Ahmadi, Y. Oshima, and J. S. Speck, "Chlorine-based dry etching of β-Ga_2O_3," *Semicond. Sci. Technol.*, vol. 31, no. 6, p. 065006, Apr. 2016.

[17] S. Jang *et al.*, "A comparative study of wet etching and contacts on and (010) oriented β-Ga_2O_3," *J. Alloys Compounds*, vol. 731, pp. 118–125, Jan. 2018.

[18] H. Fu, Z. Lu, X. Huang, H. Chen, and Y. Zhao, "Crystal orientation dependent intersubband transition in semipolar AlGaN/GaN single quantum well for optoelectronic applications," *J. Appl. Phys.*, vol. 119, no. 17, p. 174502, May 2016.

[19] H. Chen, H. Fu, Z. Lu, X. Huang, and Y. Zhao, "Optical properties of highly polarized InGaN light-emitting diodes modified by plasmonic metallic grating," *Opt. Express*, vol. 24, no. 10, pp. A856–A867, Apr. 2016.

[20] H. Fu *et al.*, "Study of low-efficiency droop in semipolar $(20\bar{2}\bar{1})$ InGaN light-emitting diodes by time-resolved photoluminescence," *J. Display Technol.*, vol. 12, no. 7, pp. 736–741, Jul. 2016.

[21] X. Huang *et al.*, "Nonpolar and semipolar InGaN/GaN multiple-quantum-well solar cells with improved carrier collection efficiency," *Appl. Phys. Lett.*, vol. 110, no. 16, p. 161105, Apr. 2017.

[22] H. Fu, X. Huang, H. Chen, Z. Lu, X. Zhang, and Y. Zhao, "Effect of buffer layer design on vertical GaN-on-GaN p-n and Schottky power diodes," *IEEE Electron Device Lett.*, vol. 38, no. 6, pp. 763–766, Jun. 2017.

[23] M. Kasu *et al.*, "Crystal defects observed by the etch-pit method and their effects on Schottky-barrier-diode characteristics on $(\bar{2}01)$ β-Ga_2O_3," *Jpn. J. Appl. Phys.*, vol. 56, no. 9, p. 091101, Jul. 2017.

[24] P. Reddy *et al.*, "The effect of polarity and surface states on the Fermi level at III-nitride surfaces," *J. Appl. Phys.*, vol. 116, no. 12, p. 123701, Sep. 2014.

[25] J. Yang, S. Ahn, F. Ren, S. J. Pearton, S. Jang, and A. Kuramata, "High breakdown voltage $(\bar{2}01)$ β-Ga_2O_3 Schottky rectifiers," *IEEE Electron Device Lett.*, vol. 38, no. 7, pp. 906–909, Jul. 2017.

[26] Y. Cao, R. Chu, R. Li, M. Chen, R. Chang, and B. Hughes, "High-voltage vertical GaN Schottky diode enabled by low-carbon metal-organic chemical vapor deposition growth," *Appl. Phys. Lett.*, vol. 108, no. 6, p. 062103, Feb. 2016,

[27] H. Fu, X. Huang, H. Chen, Z. Lu, I. Baranowski, and Y. Zhao, "Ultra-low turn-on voltage and on-resistance vertical GaN-on-GaN Schottky power diodes with high mobility double drift layers," *Appl. Phys. Lett.*, vol. 111, no. 15, p. 152102, Oct. 2017.

[28] J. Yang *et al.*, "High reverse breakdown voltage Schottky rectifiers without edge termination on Ga_2O_3," *Appl. Phys. Lett.*, vol. 110, no. 19, p. 192101, May 2017.

[29] K. Nomoto *et al.*, "1.7-kV and 0.55-m$\Omega\cdot$cm^2 GaN p-n diodes on bulk GaN substrates with avalanche capability," *IEEE Electron Device Lett.*, vol. 37, no. 2, pp. 161–164, Feb. 2016.

[30] B. Song, A. K. Verma, K. Nomoto, M. Zhu, D. Jena, and H. G. Xing, "Vertical Ga_2O_3 Schottky barrier diodes on single-crystal β-Ga_2O_3 $(\bar{2}01)$ substrates," in *Proc. 74th IEEE Device Res. Conf.*, Jun. 2016, pp. 1–2.

[31] S. Ahn, F. Ren, L. Yuan, S. J. Pearton, and A. Kuramata, "Temperature-dependent characteristics of Ni/Au and Pt/Au Schottky diodes on β-Ga_2O_3," *ECS J. Solid State Sci. Technol.*, vol. 6, no. 1, pp. P68–P72, Jan. 2017.

[32] A. M. Armstrong, M. H. Crawford, A. Jayawardena, A. Ahyi, and S. Dhar, "Role of self-trapped holes in the photoconductive gain of β-gallium oxide Schottky diodes," *J. Appl. Phys.*, vol. 119, no. 10, p. 103102, Mar. 2016.

[33] Y. Yao, R. Gangireddy, J. Kim, K. K. Das, R. F. Davis, and L. M. Porter, "Electrical behavior of β-Ga_2O_3 Schottky diodes with different Schottky metals," *J. Vac. Sci. Technol. B, Microelectron. Process. Phenom.*, vol. 35, no. 3, p. 03D113, May 2017.

[34] H. Fu *et al.*, "Demonstration of AlN Schottky barrier diodes with blocking voltage over 1 kV," *IEEE Electron Device Lett.*, vol. 38, no. 9, pp. 1286–1289, Sep. 2017.

[35] J. H. Werner and H. H. Güttler, "Barrier inhomogeneities at Schottky contacts," *J. Appl. Phys.*, vol. 69, no. 3, p. 1522, Feb. 1991.

[36] F. Iucolano, F. Roccaforte, F. Giannazzo, and V. Raineri, "Barrier inhomogeneity and electrical properties of Pt/GaN Schottky contacts," *J. Appl. Phys.*, vol. 102, no. 11, p. 113701, Dec. 2007.

[37] H. Fu, X. Huang, H. Chen, Z. Lu, and Y. Zhao, "Fabrication and characterization of ultra-wide bandgap AlN-based Schottky diodes on sapphire by MOCVD," *IEEE J. Electron Devices Soc.*, vol. 5, no. 6, pp. 518–524, Nov. 2014.

[38] E. J. Miller, E. T. Yu, P. Waltereit, and J. S. Speck, "Analysis of reverse-bias leakage current mechanisms in GaN grown by molecular-beam epitaxy," *Appl. Phys. Lett.*, vol. 84, no. 4, p. 535, Jan. 2004.

[39] Y. Irokawa, E. Villora, and K. Shimamura, "Shottky barrier diodes on AlN free-standing substrates," *Jpn. J. Appl. Phys.*, vol. 51, no. 4R, p. 040206, Mar. 2012.

Houqiang Fu (S'18) is currently pursuing the Ph.D. degree with the School of Electrical, Computer, and Energy Engineering, Arizona State University, Tempe, AZ, USA.

His current research interests include wide bandgap power electronics, optoelectronics, optical devices, and visible light communication.

Hong Chen is currently pursuing the Ph.D. degree with the School of Electrical, Computer, and Energy Engineering, Arizona State University, Tempe, AZ, USA.

His current research interests include wide bandgap power electronics, optoelectronics, optical devices, and visible light communication.

Xuanqi Huang is currently pursuing the Ph.D. degree with the School of Electrical, Computer, and Energy Engineering, Arizona State University, Tempe, AZ, USA.

His current research interests include wide bandgap power electronics, optoelectronics, optical devices, and visible light communication.

Izak Baranowski is currently pursuing the Ph.D. degree with the School of Electrical, Computer, and Energy Engineering, Arizona State University, Tempe, AZ, USA.

His current research interests include wide bandgap power electronics, optoelectronics, optical devices, and visible light communication.

Jossue Montes is currently pursuing the Ph.D. degree with the School of Electrical, Computer, and Energy Engineering, Arizona State University, Tempe, AZ, USA.

His current research interests include wide bandgap power electronics, optoelectronics, optical devices, and visible light communication.

Tsung-Han Yang is currently pursuing the Ph.D. degree with the School of Electrical, Computer, and Energy Engineering, Arizona State University, Tempe, AZ, USA.

His current research interests include wide bandgap power electronics, optoelectronics, optical devices, and visible light communication.

Yuji Zhao (M'14) received the Ph.D. degree in electrical and computer engineering from the University of California at Santa Barbara, Santa Barbara, CA, USA, in 2012.

He is currently an Assistant Professor with Arizona State University, Tempe, AZ, USA. His current research interests include advanced electronic and optoelectronic devices based on wide bandgap semiconductors.